arXiv:1605.08886v1 [cond-mat.mtrl-sci] 28 May 2016

Potential thermoelectric materials $CsMI_3$ (M=Sn and Pb) in perovskite structures from the first-principles calculations

San-Dong Guo and Jian-Li Wang
Department of Physics, School of Sciences, China University of Mining and Technology, Xuzhou 221116, Jiangsu, China

The thermoelectric properties of halide perovskites $CsMI_3$ (M=Sn and Pb) are investigated from a combination of first-principles calculations and semiclassical Boltzmann transport theory by considering both the electron and phonon transport. The electronic part is performed using a modified Becke and Johnson (mBJ) exchange potential, including spin-orbit coupling (SOC), while the phonon part is computed using generalized gradient approximation (GGA). It is found that SOC has remarkable detrimental effect on n-type power factor, while has a negligible influence in p-type doping, which can be explained by considering SOC effect on conduction and valence bands. Calculated results show exceptionally low lattice thermal conductivities in $CsSnI_3$ and $CsPbI_3$, and the corresponding room-temperature lattice thermal conductivity is 0.54 $Wm^{-1}K^{-1}$ and 0.25 $Wm^{-1}K^{-1}$. At 1000 K, the maximal figure of merit ZT is up to 0.63 and 0.64 for $CsSnI_3$ and $CsPbI_3$ with scattering time τ=10^{-14} s, and the peak ZT is 0.49 and 0.41 with τ=10^{-15} s. These results make us believe that $CsMI_3$ (M=Sn and Pb) in perovskite structures may be potential thermoelectric materials.

PACS numbers: 72.15.Jf, 71.20.-b, 71.70.Ej, 79.10.-n
Keywords: Perovskites; Spin-orbit coupling; Power factor; Thermal conductivity

I. INTRODUCTION

Thermoelectric materials enable the direct conversion from heat to electricity, which may make essential contributions to the crisis of energy[1,2]. A good thermoelectric material should have high dimensionless figure of merit $ZT = S^2\sigma T/(\kappa_e + \kappa_L)$, where S, σ, T, κ_e and κ_L are the Seebeck coefficient, electrical conductivity, absolute temperature, the electronic and lattice thermal conductivities, respectively. A high ZT material requires high power factor ($S^2\sigma$) and low thermal conductivity ($\kappa = \kappa_e + \kappa_L$). They generally influence each other, and a counteracted relationship between electrical conductivity and thermal conductivity or Seebeck coefficient is often found. The excellent classic thermoelectric materials include bismuth-tellurium systems[3,4], silicon-germanium alloys[5,6], lead chalcogenides[7,8] and skutterudites[9,10]. For thermoelectric research, searching for potential high ZT materials with classic common lattice structure, like perovskite structure, is interesting and challenging.

The cubic perovskite structure $SrTiO_3$ has attracted growing attention for thermoelectric power generation[11]. The ZT value of undoped $SrTiO_3$ is less than 0.5 due to its high thermal conductivity[12], which can be reduced by introducing point defects[13,14]. Searching other perovskites for more efficient thermoelectric applications is imperative and amusing. Hybrid AMX_3 perovskites (A=Cs, CH_3NH_3; M=Sn, Pb; X=halide) have recently attracted a great deal of attention for solar cell designs, which can realize up to 15% energy conversion efficiencies[15–18]. A fair amount of theoretical works have been performed to investigate their electronic structures, phonons and optical properties[19–24]. The $CsMI_3$ (M=Sn and Pb) of them under reasonable hydrostatic pressure can turn into three-dimensional topological insulators, which has been predicted by first-principles calculations[25,26].

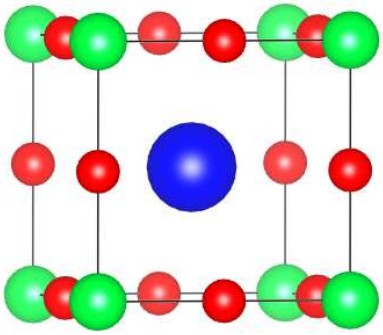

FIG. 1. (Color online) The crystal structure of $CsMI_3$ (M=Sn and Pb). The largest blue ball represent Cs atom, the medium green balls X, and the smallest red balls I.

Here, we report on the thermoelectric properties of cubic $CsMI_3$ (M=Sn and Pb) in perovskite structures from a combination of first-principles calculations and semiclassical Boltzmann transport theory. The SOC can produce obvious effects on power factor of many thermoelectric materials[27–34], so the SOC is included in our calculations of electronic part. Calculated results show SOC has a noteworthy reduced influence for n-type power factor. It is noteworthy that ultralow lattice thermal conductivities are attained for $CsMI_3$ (M=Sn and Pb), and the corresponding lattice thermal conductivity at 300 K is 0.54 $Wm^{-1}K^{-1}$ and 0.25 $Wm^{-1}K^{-1}$, which is compared with lattice thermal conductivity of 0.23 $Wm^{-1}K^{-1}$ in SnSe with an unprecedented ZT of 2.6 at 923 K[35]. Finally, the dimensionless thermoelectric figure of merit ZT is calculated with τ=10^{-14} s or τ=10^{-15} s , and can be up to about 0.6 or 0.4 at high temperature by the optimized doping.

The rest of the paper is organized as follows. In the

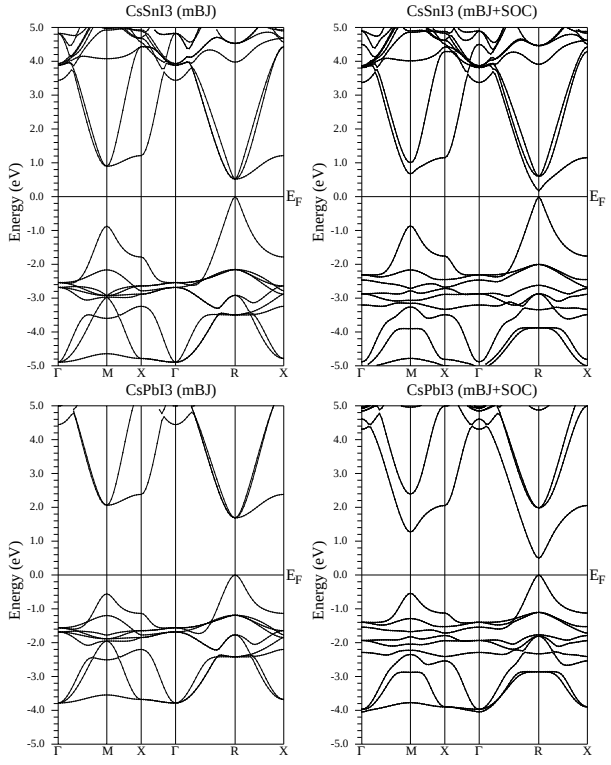

FIG. 2. The energy band structures of $CsMI_3$ (M=Sn and Pb) using mBJ (Left) and mBJ+SOC (Right).

next section, we shall describe computational details. In the third section, we shall present the electronic structures and thermoelectric properties of $CsMI_3$ (M=Sn and Pb). Finally, we shall give our discussions and conclusion in the fourth section.

II. COMPUTATIONAL DETAIL

The electronic structures of $CsMI_3$ (M=Sn and Pb) are performed using a full-potential linearized augmented-plane-waves method within the density functional theory (DFT)[36], as implemented in the WIEN2k package[37]. We employ Tran and Blaha's mBJ exchange potential plus local-density approximation (LDA) correlation potential for the exchange-correlation potential[38], which has been known to produce more accurate band gaps than LDA and GGA. The SOC was included self-consistently[39–42] due to containing heavy elements, which leads to band splitting, and produces important effects on power factor. We use 5000 k-points in the first Brillouin zone for the self-consistent calculation, make harmonic expansion up to $l_{max} = 10$ in each of the atomic spheres, and set $R_{mt} * k_{max} = 8$. The self-consistent calculations are considered to be converged when the integration of the absolute charge-density difference between the input and output electron density is less than $0.0001|e|$ per formula unit, where e is the electron charge. Transport calculations, including Seebeck coefficient, electrical conductivity and electronic thermal conductivity, are performed through solving Boltzmann transport equations within the constant scattering time approximation (CSTA) as implemented in BoltzTrap[43], and reliable results have been obtained for several materials[44–46]. To obtain accurate transport coefficients, we use 140000 k-points in the first Brillouin zone for the energy band calculation. The lattice thermal conductivities are calculated within the linearized phonon Boltzmann equation by using Phono3py+VASP codes[47–50]. For the third-order force constants, 2×2×2 supercells are built, and reciprocal spaces of the supercells are sampled by 3×3×3 meshes. To compute lattice thermal conductivities, the reciprocal spaces of the primitive cells are sampled using the 20×20×20 meshes.

III. MAIN CALCULATED RESULTS AND ANALYSIS

$CsMI_3$ (M=Sn and Pb) belong to perovskite semiconductors, which consists of a network of corner-sharing MI_6 octahedra, and the schematic crystal structure is shown in Figure 1. Based on the experimental structures, the electronic structures of $CsMI_3$ (M=Sn and Pb) are investigated using mBJ and mBJ+SOC, and the energy band structures are plotted in Figure 2. Both mBJ and mBJ+SOC show $CsMI_3$ (M=Sn and Pb) are direct-gap semiconductor, with the conduction band minimum (CBM) and valence band maximum (VBM) at the R point. The mBJ and mBJ+SOC energy band gap values are 0.52 eV (1.69 eV) and 0.17 eV (0.50 eV) for $CsSnI_3$ ($CsPbI_3$), respectively. The conduction bands are dominated by M-6p states, and the CBM is threefold degenerate at the absence of SOC. The VBM is a mixture of I-p and M-s states, which is nondegenerate. The SOC can remove band degeneracy, and leads to a spin-orbital splitting value of 0.43 eV and 1.49 eV for $CsSnI_3$ and $CsPbI_3$ at CBM. It is clearly seen that, near the Fermi level, the SOC has more obvious influence on the conduction bands than on the valence bands. The related data are shown in Table I, and the mBJ gaps are larger than GGA or LDA ones, but are less than GW or HSE ones[19,21–24].

TABLE I. The experimental lattice constant a (Å); the calculated energy band gap values with mBJ E_1 (eV) and mBJ+SOC E_2 (eV); $E_1 - E_2$ (eV); spin-orbit splitting Δ (eV) at the CBM.

Name	a	E_1	E_2	$E_1 - E_2$	Δ
$CsSnI_3$	6.22	0.52	0.17	0.35	0.43
$CsPbI_3$	6.29	1.69	0.50	1.19	1.49

Next, we calculate semi-classic transport coefficients using CSTA Boltzmann theory. The rigid band approach is used to mimic the doping effects by shifting

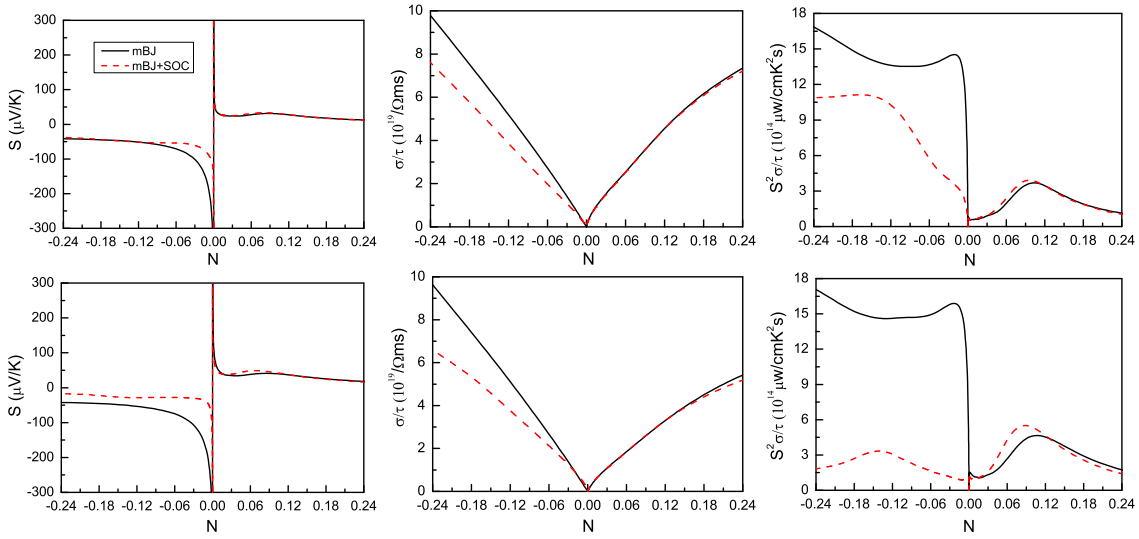

FIG. 3. (Color online) At room temperature, transport coefficients of $CsSnI_3$ (Top panel) and $CsPbI_3$ (Bottom panel) as a function of doping level (N): Seebeck coefficient S, electrical conductivity with respect to scattering time σ/τ and power factor with respect to scattering time $S^2\sigma/\tau$ calculated with mBJ (Black solid lines) and mBJ+SOC (Red dash lines). The N means electrons (minus value) or holes (positive value) per unit cell.

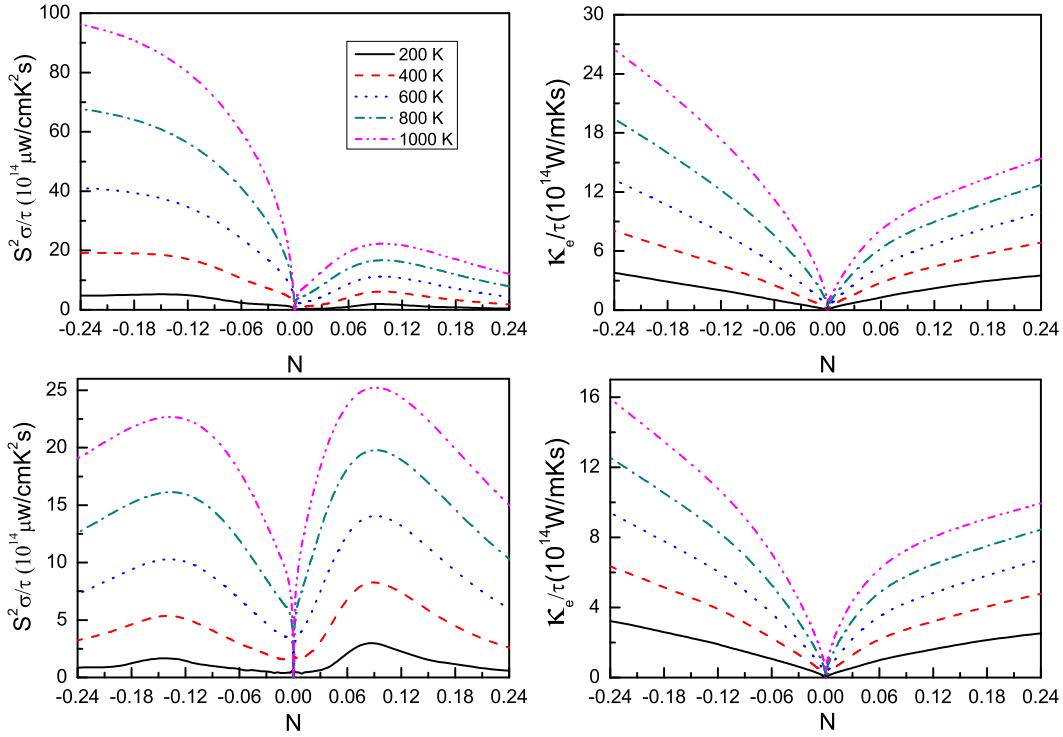

FIG. 4. (Color online) The power factor with respect to scattering time $S^2\sigma/\tau$ and electronic thermal conductivity with respect to scattering time κ_e/τ of $CsSnI_3$ (Top panel) and $CsPbI_3$ (Bottom panel) as a function of doping level with temperature being 200, 400, 600 , 800 and 1000 (unit: K) using mBJ+SOC.

the Fermi level, which is reasonable, when the doping level is low[51–53]. The semi-classic transport coefficients, such as Seebeck coefficient S, electrical conductivity with respect to scattering time σ/τ and power factor with respect to scattering time $S^2\sigma/\tau$, as a function of doping level at room temperature using mBJ and mBJ+SOC are plotted in Figure 3. Due to electrical thermal conductivity $\kappa_e = L\sigma T$ (Lorenz number $L = \pi^2 k_B^2/3e^2$, where K_B is the Boltzmann constant, e is the charge of an electron.), the electrical thermal conductivity has similar outlines

TABLE II. Peak ZT for both n- and p-type at 1000 K with τ=10^{-14} s and τ=10^{-15} s, and the corresponding doping concentrations. The doping concentration equals 4.16×10^{21}cm^{-3}(4.02×10^{21}cm^{-3})× doping level for $CsSnI_3$ ($CsPbI_3$).

	τ=10^{-14} s				τ=10^{-15} s			
	n		p		n		p	
Name	(×10^{19}cm^{-3})	ZT	(×10^{19}cm^{-3})	ZT	(×10^{19}cm^{-3})	ZT	(×10^{19}cm^{-3})	ZT
$CsSnI_3$	4.16	0.63	1.08	0.36	9.78	0.49	1.88	0.19
$CsPbI_3$	0.53	0.64	0.60	0.65	1.14	0.38	1.53	0.41

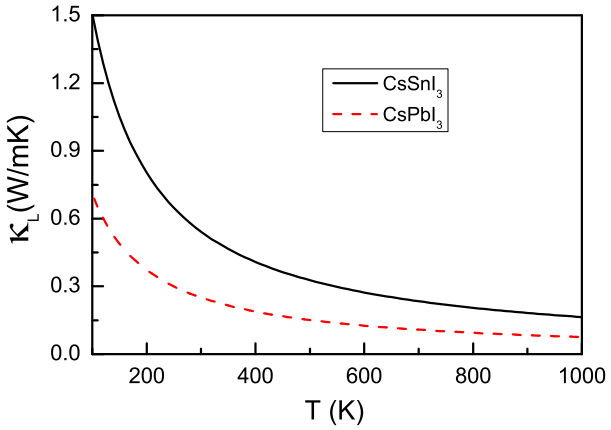

FIG. 5. (Color online) The lattice thermal conductivities κ_L of $CsMI_3$ (M=Sn and Pb) as a function of temperature using GGA.

with electrical conductivity. The Fermi level moves into conduction bands, which means n-type doping (negative doping levels) with the negative Seebeck coefficient. The p-type doping (positive doping levels) with the positive Seebeck coefficient can be achieved by shifting Fermi level into the valence bands. Although the Seebeck coefficient is very large, when the Fermi level is in the middle of band gap, the low electrical conductivity leads to very small power factor. Shifting the Fermi level into conduction bands or valence bands, the Seebeck coefficient (absolute value) decreases, while the electrical conductivity increases, which leads to a maximum of power factor at certain doping level.

It has been proved that SOC has very important effects on power factor in many thermoelectric materials containing heavy elements[27–34]. Calculated results show that SOC has obvious reduced influences on S and σ/τ in n-type doping for both $CsSnI_3$ and $CsPbI_3$, but weak effects for p-type. The large slope of density of states (DOS) near the energy band gap can induce a large Seebeck coefficient in narrow-gap semiconductors. This can be understood by the following formula: $S = \frac{\pi^2}{3}(\frac{k_B^2 T}{e})[\frac{1}{n}\frac{dn(E)}{dE} + \frac{1}{\mu}\frac{d\mu(E)}{dE}]_{E=E_f}$ [54], where $n(E)$ and $\mu(E)$ are energy dependent carrier density and mobility, respectively. It is found that the slope of DOS using mBJ near the energy band gap is larger than that using mBJ+SOC for conduction bands, while they are nearly the same for valence bands. Band degeneracy, namely band convergence, can induce lager slope of DOS. The SOC can reduce the slope of DOS by removing band degeneracy. The SOC effects on energy bands can explain SOC influences on S. The SOC-induced reduced S and σ/τ for n-type lead to a very remarkable detrimental influence on power factor, especially for $CsPbI_3$. However, the SOC has weak effects on p-type power factor. For $CsPbI_3$, at the absence of SOC, the best n-type power factor is larger than that in p-type doping. However, including SOC, it is opposite in considered doping range. Similar SOC-induced switch of best power factor between n-type and p-type can be achieved in Mg_2Sn[32]. Therefore, including SOC is very important in the theoretical prediction of thermoelectric properties of $CsMI_3$ (M=Sn and Pb).

The power factor and electronic thermal conductivity with respect to scattering time ($S^2\sigma/\tau$ and κ_e/τ) of $CsSnI_3$ and $CsPbI_3$ as a function of doping level with temperature from 200 K to 1000 K using mBJ+SOC are shown in Figure 4. For $CsSnI_3$, n-type doping has larger power factor than p-type doping, while p-type power factor is larger than n-type one for $CsPbI_3$. if we assume scattering time is constant, in considered doping and temperature range, the best power factor of $CsSnI_3$ is nearly four times larger than one of $CsPbI_3$, and about two times larger for electronic thermal conductivity. The lattice thermal conductivity is important factor, which significantly affects thermoelectric performance. The lattice thermal conductivities κ_L of $CsMI_3$ (M=Sn and Pb) as a function of temperature are shown in Figure 5. Calculated results show ultralow lattice thermal conductivities in $CsMI_3$ (M=Sn and Pb). The lattice thermal conductivity can be assumed to have weak dependence on doping level, and typically goes as 1/T. The corresponding room-temperature lattice thermal conductivity is 0.54 Wm^{-1}K^{-1} and 0.25 Wm^{-1}K^{-1} for $CsSnI_3$ and $CsPbI_3$. Theoretically, ultralow lattice thermal conductivities in many compounds have been predicted, such as $PbRbI_3$ (0.10 Wm^{-1}K^{-1}), PbIBr (0.13 Wm^{-1}K^{-1}) and K_2CdPb (0.45 Wm^{-1}K^{-1})[55]. It is found that lattice thermal conductivity of $CsSnI_3$ is nearly two times larger than one of $CsPbI_3$.

Due to the complexity of various carrier scattering mechanisms, it is difficult to calculate scattering time τ from the first principles. To estimate thermoelectric conversion efficiency, the thermoelectric figure of merit ZT

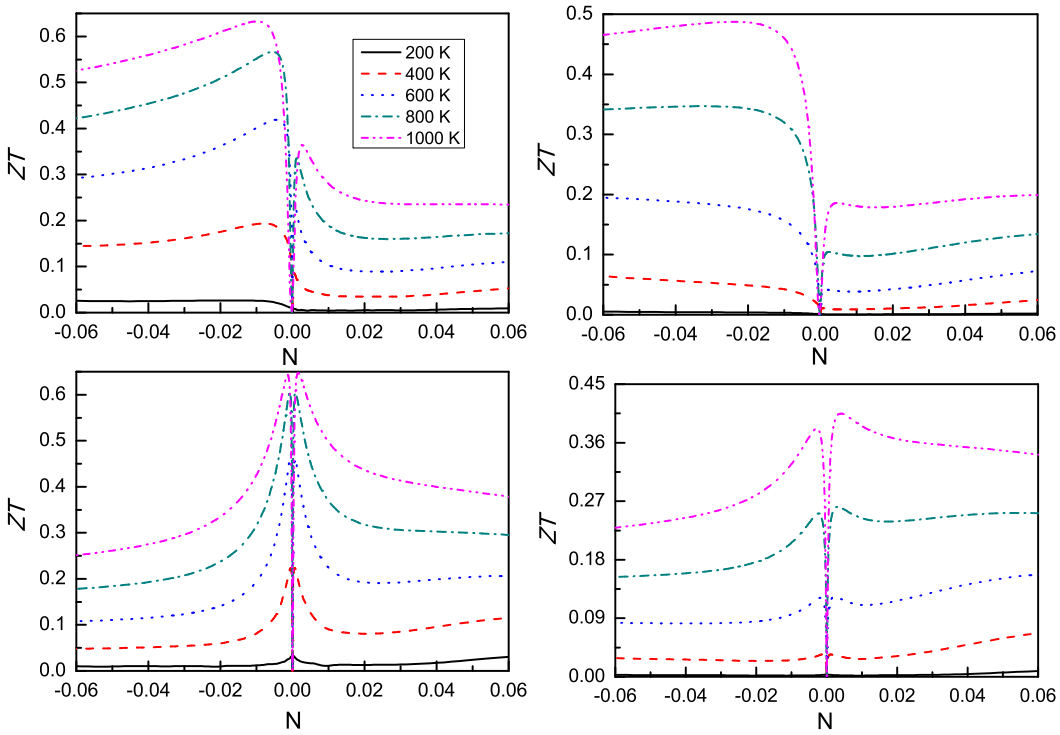

FIG. 6. (Color online) The ZT of $CsSnI_3$ (Top panel) and $CsPbI_3$ (Bottom panel) as a function of doping level with temperature being 200, 400, 600 , 800 and 1000 (unit: K), and the scattering time τ is 1×10^{-14} s (Left) and 1×10^{-15} s (Right).

is calculated with hypothetical τ=10^{-14} and τ=10^{-15} s, and are plotted in Figure 6. The peak ZT and corresponding doping concentrations for both n- and p-type at 1000 K are summarized in Table II. For $CsSnI_3$, the n-type doping has larger ZT than p-type doping, which is mainly due to the larger n-type Seebeck coefficient. However, the ZT between n- and p-type are nearly the same for $CsPbI_3$ due to almost the same Seebeck coefficient. According to Figure 4 and Figure 5, the total thermal conductivity κ is dominated by the lattice thermal conductivity κ_L in the very low doping level, but the electronic thermal conductivity κ_e becomes very larger than lattice thermal conductivity κ_L in slightly high doping region. These leads to very low doping concentration for peak ZT. Therefore, electronic thermal conductivity of $CsMI_3$ (M=Sn and Pb) is a fatal disadvantage to gain more higher ZT value.

IV. DISCUSSIONS AND CONCLUSION

The CBM of $CsMI_3$ (M=Sn and Pb) is dominated by a giant spin-orbit coupling (SOC), especially for $CsPbI_3$. The SOC removes the band degeneracy of CBM by spin-orbit splitting, which leads to obvious effects on n-type Seebeck coefficient, and further affects the power factor. The larger spin-orbit splitting Δ leads to the more obvious detrimental influence on n-type power factor, which can be observed from Figure 4. The similar SOC-induced detrimental influence on power factor has been observed in Mg_2Sn and half-Heusler ANiB (A=Ti, Hf, Sc, Y; B=Sn, Sb, Bi)[28,32]. Therefore, it is very important for electronic part of thermoelectric properties of $CsMI_3$ (M=Sn and Pb) to include SOC.

$CsMI_3$ (M=Sn and Pb) have been predicted to be three-dimensional topological insulators under reasonable hydrostatic pressure using a tight-binding analysis and first-principles calculations[25,26], which means that the electronic structures of $CsMI_3$ (M=Sn and Pb) are easily tuned by pressure. Pressure-induced enhanced power factor has been predicted in Mg_2Sn[32] and BiTeI[56] by the first-principles calculations. Experimentally, it is possible to tune the thermoelectric properties of $CsMI_3$ (M=Sn and Pb) by pressure.

In summary, mBJ and mBJ+SOC are chosen to investigate electronic structures and electronic part of thermoelectric properties of halide perovskites $CsMI_3$ (M=Sn and Pb). The strength of SOC influences on CBM is very large, especially for $CsPbI_3$, which gives rise to obvious detrimental influence on n-type power factor. The lattice thermal conductivities of $CsMI_3$ (M=Sn and Pb) are performed with GGA, and ultralow lattice thermal conductivities are predicted, which is very key for providing high thermoelectric performance. At 1000 K, in low doping level, the figure of merit ZT is up to about 0.6 with τ=10^{-14}, and about 0.4 with τ=10^{-15}. The present work provides a platform to search potential thermoelectric materials from perovskite compounds.

ACKNOWLEDGMENTS

This work is supported by the National Natural Science Foundation of China (Grant No. 11404391). We are grateful to the Advanced Analysis and Computation Center of CUMT for the award of CPU hours to accomplish this work.

[1] Y. Pei, X. Shi, A. LaLonde, H. Wang, L. Chen and G. J. Snyder, Nature **473**, 66 (2011).
[2] L. E. Bell, Science **321**, 1457 (2008).
[3] W. S. Liu, Q. Y. Zhang, Y. C. Lan, S. Chen, X. Yan, Q. Zhang, H. Wang, D. Z. Wang, G. Chen and Z. F. Ren, Adv. Energy Mater. **1**, 577 (2011).
[4] D. K. Ko, Y. J. Kang and C. B. Murray, Nano Lett., **11**, 2841 (2011).
[5] M. Zebarjadi, et al. Nano Lett. **11**, 2225 (2011).
[6] B. Yu, et al. Nano Lett. **12**, 2077 (2012).
[7] Y. Z. Pei, X. Y. Shi, A. Lalonde et al, Nature **473**, 66 (2011).
[8] J. Q. He, J. R. Sootsman, S. N. Girard et al, J. Am. Chem. Soc. **132**, 8669 (2010).
[9] A. C. Sklad, M. W. Gaultois and A. P. Grosvenor, J. Alloys Compd. **505**, L6 (2010).
[10] X. Shi, J. Yang and J. R. Salvador, J. Am. Chem. Soc. **133**, 7837 (2011).
[11] T. Okuda, K. Nakanishi, S. Miyasaka, and Y. Tokura, Phys. Rev. B **63**, 113104 (2001).
[12] H. Muta, K. Kurosaki, and S. Yamanaka, J. Alloys Compd **392**, 306 (2005)
[13] S. Ohta, T. Nomura, H. Ohta, and K. Koumoto, J. Appl. Phys. **97**, 034106 (2005).
[14] H. C. Wang, C. L. Wang, W. B. Su, J. Liu, Y. Sun, H. Peng, and L. M. Mei, J. Am. Ceram. Soc. **94**, 838 (2011).
[15] J. Burschka, N. Pellet, S.-J. Moon, R. Humphry-Baker, P. Gao, M. K. Nazeeruddin, and M. Grätzel, Nature **499**, 316 (2013).
[16] M. Liu, M. B. Johnston, and H. J. Snaith, Nature **501**, 395 (2013).
[17] K. Wojciechowski, M. Saliba, T. Leijtens, A. Abate, and H. J. Snaith, Energy Environ. Sci. **7**, 1142 (2014).
[18] G. Hodes, Science **342**, 317 (2013).
[19] P. Umari, E. Mosconi and F. De Angelis, Sci. Rep. **4**, 4467 (2014).
[20] L. Y. Huang and Walter R. L. Lambrecht, Phys. Rev. B **90**, 195201 (2014).
[21] L. Y. Huang and Walter R. L. Lambrecht, Phys. Rev. B **88**, 165203 (2013).
[22] J. Even, L. Pedesseau, J. M. Jancu and C. Katan, Phys. Status Solidi RRL **8** 31 (2014).
[23] J. Even, L. Pedesseau, J. M. Jancu and C. Katan, J. Phys. Chem. Lett **4**, 2999 (2013).
[24] L. Lang, J. H.Yang, H. R. Liu, H. J. Xiang and X. G. Gong, Phys. Lett. A **378**, 290 (2014).
[25] K. Yang, W. Setyawan, S. Wang, M. B. Nardelli and S. Curtarolo, Nat. Mater. **11**, 614 (2012).
[26] H. Jin, J. Im and A. J. Freeman, Phys. Rev. B **86**, 121102 (2012).
[27] K. Kutorasinski, B. Wiendlocha, J. Tobola and S. Kaprzyk, Phys. Rev. B **89**, 115205 (2014).
[28] S. D. Guo, J. Alloy. Compd. **663**, 128 (2016).
[29] P. Larson, S. D. Mahanti, and M. G. Kanatzidis, Phys. Rev. B **61**, 8162 (2000).
[30] T. J. Scheidemantel, C. Ambrosch-Draxl, T. Thonhauser, J. V. Badding, and J. O. Sofo, Phys. Rev. B **68**, 125210 (2003).
[31] S. J. Youn and A. J. Freeman, Phys. Rev. B **63**, 085112 (2001).
[32] S. D. Guo and J. L. Wang, RSC Adv. **6**, 31272 (2016).
[33] S. D. Guo, RSC Adv. **6**, 47953 (2016).
[34] N. Singh and U. Schwingenschlögl, Phys. Status Solidi RRL **08**, 805 (2014).
[35] L. D. Zhao, S. H. Lo, Y. S. Zhang et al, Nature **508**, 373 (2014).
[36] P. Hohenberg and W. Kohn, Phys. Rev. **136**, B864 (1964); W. Kohn and L. J. Sham, Phys. Rev. **140**, A1133 (1965).
[37] P. Blaha, K. Schwarz, G. K. H. Madsen, D. Kvasnicka and J. Luitz, WIEN2k, an Augmented Plane Wave + Local Orbitals Program for Calculating Crystal Properties (Karlheinz Schwarz Technische Universität Wien, Austria) 2001, ISBN 3-9501031-1-2
[38] F. Tran and P. Blaha, Phys. Rev. Lett. **102**, 226401 (2009).
[39] A. H. MacDonald, W. E. Pickett and D. D. Koelling, J. Phys. C **13**, 2675 (1980).
[40] D. J. Singh and L. Nordstrom, Plane Waves, Pseudopotentials and the LAPW Method, 2nd Edition (Springer, New York, 2006).
[41] J. Kunes, P. Novak, R. Schmid, P. Blaha and K. Schwarz, Phys. Rev. B **64**, 153102 (2001).
[42] D. D. Koelling, B. N. Harmon, J. Phys. C Solid State Phys. **10**, 3107 (1977).
[43] G. K. H. Madsen and D. J. Singh, Comput. Phys. Commun. **175**, 67 (2006).
[44] B. L. Huang and M. Kaviany, Phys. Rev. B **77**, 125209 (2008).
[45] L. Q. Xu, Y. P. Zheng and J. C. Zheng, Phys. Rev. B **82**, 195102 (2010).
[46] J. J. Pulikkotil, D. J. Singh, S. Auluck, M. Saravanan, D. K. Misra, A. Dhar and R. C. Budhani, Phys. Rev. B **86**, 155204 (2012).
[47] G. Kresse, J. Non-Cryst. Solids **193**, 222 (1995).
[48] G. Kresse and J. Furthmüller, Comput. Mater. Sci. 6, **15** (1996).
[49] G. Kresse and D. Joubert, Phys. Rev. B **59**, 1758 (1999).
[50] A. Togo, L. Chaput and I. Tanaka, Phys. Rev. B **91**, 094306 (2015).
[51] T. J. Scheidemantel, C. Ambrosch-Draxl, T. Thonhauser, J. V. Badding and J. O. Sofo, Phys. Rev. B **68**, 125210 (2003).
[52] G. K. H. Madsen, J. Am. Chem. Soc. **128**, 12140 (2006).
[53] X. Gao, K. Uehara, D. Klug, S. Patchkovskii, J. Tse and T. Tritt, Phys. Rev. B **72**, 125202 (2005).

[54] W. Liu, X. Tan, K. Yin, H. Liu, X. Tang, J. Shi, Q. Zhang and C. Uher, Phys. Rev. Lett. **108**, 166601 (2012).
[55] A. Seko, A. Togo, H. Hayashi, K. Tsuda, L. Chaput and I. Tanaka, Phys. Rev. Lett. **115**, 205901 (2015).
[56] S. D. Guo and J. L. Wang, J. Phys. D: Appl. Phys. **49**, 215107 (2016).